

# International Conference on Space Optics—ICSO 2014

La Caleta, Tenerife, Canary Islands

7–10 October 2014

*Edited by Zoran Sodnik, Bruno Cugny, and Nikos Karafolas*



## *A deployable telescope for sub-meter resolutions from microsatellite platforms*

*D. Dolkens*

*J. M. Kuiper*



icso proceedings



## A DEPLOYABLE TELESCOPE FOR SUB-METER RESOLUTIONS FROM MICROSATELLITE PLATFORMS

D. Dolkens and J. M. Kuiper  
*Delft University of Technology, the Netherlands*  
*Kluyverweg 1, 2629 HS Delft*  
*dd@spaceoptics.eu*

**Abstract** - Sub-meter resolution imagery has become increasingly important for disaster response, defence and security applications. Earth Observation (EO) at these resolutions has long been the realm of large and heavy telescopes, which results in high image costs, limited availability and long revisit times. Using synthetic aperture technology, instruments can now be developed that can reach these resolutions using a substantially smaller launch volume and mass.

To obtain a competitive MicroSatellite telescope design, a concept study was performed to develop a deployable instrument that can reach a ground resolution of 25 cm from an orbital altitude of 500 km. Two classes of instruments were analysed: the Fizeau synthetic aperture, a telescope that uses a segmented primary mirror, and a Michelson synthetic aperture, an instrument concept that combines the light of a distributed array of afocal telescopes into a final image. In a trade-off the Fizeau synthetic aperture was selected as the most promising concept for obtaining high resolution imagery from a Low Earth Orbit.

The optical design of the Fizeau synthetic aperture is based on a full-field Korsch telescope that has been optimized for compactness and an excellent wavefront quality. It uses three aperture segments in a tri-arm configuration that can be folded alongside the instrument during launch. The secondary mirror is mounted on a deployable boom, further decreasing the launch volume.

To maintain a high image quality while operating in the harsh and dynamic space environment, one of the most challenging obstacles that must be addressed is the very tight tolerance on the positioning of the three primary mirror segments and the secondary mirror. Following a sensitivity analysis, systems engineering budgets have been defined.

The instrument concept features a robust thermo-mechanical design, aimed at reducing the mechanical uncertainties to a minimum. Silicon Carbide mirror segments, the use of Invar for the deployable arms and a main housing with active thermal control, will guarantee a high thermal stability during operations.

Since a robust mechanical design alone is insufficient to ensure a diffraction limited performance, an in-orbit calibration system was developed. Post launch, a combination of interferometric measurements and capacitive sensors will be used to characterise the system. Actuators beneath the primary mirror segments will then correct the position of the mirror segments to meet the required operating accuracies. During operations, a passive system will be used. This system relies on a phase diversity algorithm to retrieve residual wavefront aberrations and deconvolve the image data. Using this approach, a good end-to-end imaging performance can be achieved.

### I. INTRODUCTION

Over the last decades, high resolution satellite data has become increasingly embedded in modern society. Detailed images of the Earth play a more and more important role in fields such as defence and security, disaster prevention and environmental monitoring. Thanks to applications such as Google Maps, high resolution satellite images are just a few mouse clicks away.

Presently, high resolution satellite data is captured by Earth Observation (EO) systems such as GeoEye, Quickbird, Worldview and Spot. Such satellites are large, heavy and expensive. As a result, data produced by these satellite systems is also very expensive. Moreover, the number of systems capable of capturing imagery at a high resolution is still limited whilst the swath width of these systems is typically small. This means that for many regions on Earth, frequently updated imagery is simply not available.

The goal was therefore set to design a deployable optical system that can reach similar resolutions as state-of-the-art EO systems, while using a fraction of the volume and mass. The launch costs of such a system are substantially smaller, which will ultimately result in a much lower cost per image.

In table 1, the main optical properties are listed that have been used as a starting point for the design. The ground resolution target and orbital altitude were derived from the Worldview-3 specifications, the recently launched 2800 kg EO satellite [1].

**Table 1:** Main Optical Properties

<i>Pupil Baseline</i>		1.5 m
<i>Focal Length</i>		11 m
<i>Orbital Altitude</i>		500 km
<i>Swath Width</i>		5 km
<i>Field of View</i>		0.57°
<i>Aperture Area</i>		0.65 m <sup>2</sup>
<i>GSD</i>	<i>Panchromatic (450-650 nm)</i>	25 cm
	<i>Blue (450-510 nm)</i>	100 cm
	<i>Green (520-580 nm)</i>	100 cm
	<i>Yellow (580-630 nm)</i>	100 cm
	<i>Red (630 – 700 nm)</i>	100 cm

## II. OPTICAL CONCEPTS AND TRADE-OFF

There are two main approaches which can followed when designing a synthetic aperture instrument [2]:

- **Michelson Synthetic Aperture:** For this class of instruments, the light is collected by a number of afocal telescopes that are spread out over the baseline. The collimated beams of light are relayed towards a beam combiner, which focusses the light of each telescope onto a common image plane.
- **Fizeau Synthetic Aperture:** this type of synthetic aperture instrument is very similar to a conventional telescope. The main difference is that primary mirror has been split up in a number of smaller segments, which are folded alongside the instrument during launch.

During the study, conceptual designs have been created for both the Michelson and Fizeau synthetic aperture systems, which are described in subsections A and B, respectively. A trade-off between the two concepts is presented in subsection C.

### A. Michelson

The Michelson synthetic aperture concept consists of 12 afocal telescopes which are distributed in an annular configuration across the pupil plane. Each afocal telescope has an aperture diameter of 250 mm and an obscuration ratio of 0.4. The angular magnification of the telescopes is 5x. As a beam combiner, a full-field Korsch design was chosen. Glass components were deliberately avoided as chromatic aberrations will complicate the image processing algorithms that are needed to obtain a good image quality.

To ensure that the system can deliver a good performance over a wide field of view (FOV), a number of requirements must be met [3]. First of all, both the afocal telescopes and the beam combiner have to be designed to produce a diffraction limited image quality over the full FOV. Secondly, the principle of homothetic mapping must be applied, i.e. the entrance pupil of the beam combiner should be an exact demagnification of the entrance pupil of the array of telescopes.

Finally, the afocal telescopes must be designed to produce a specified amount of distortion, known as sine-law distortion. As described in [4] this ensures that for off-axis fields, the wavefronts originating from each telescope remain in phase.

To ensure that the distortion requirements could be met, without sacrificing the wavefront quality, the afocal telescopes use aspheric mirrors (even aspheres with 4 higher order terms). In Fig. 1, a three dimensional view and a cross-section of the concept are shown.

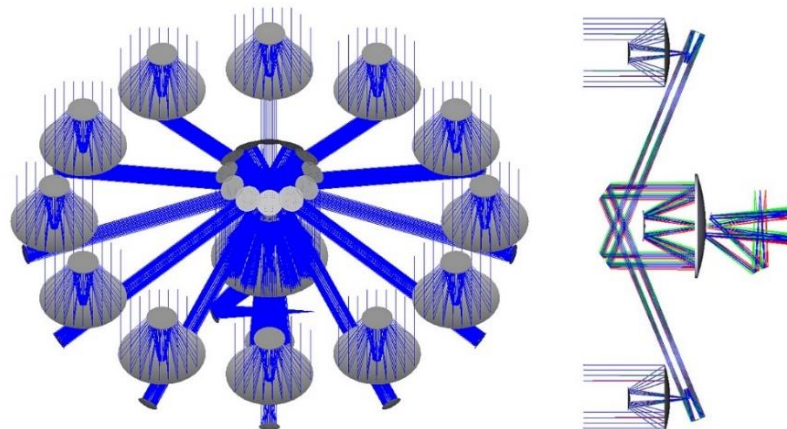


**Fig. 1:** Michelson Synthetic Aperture Concept

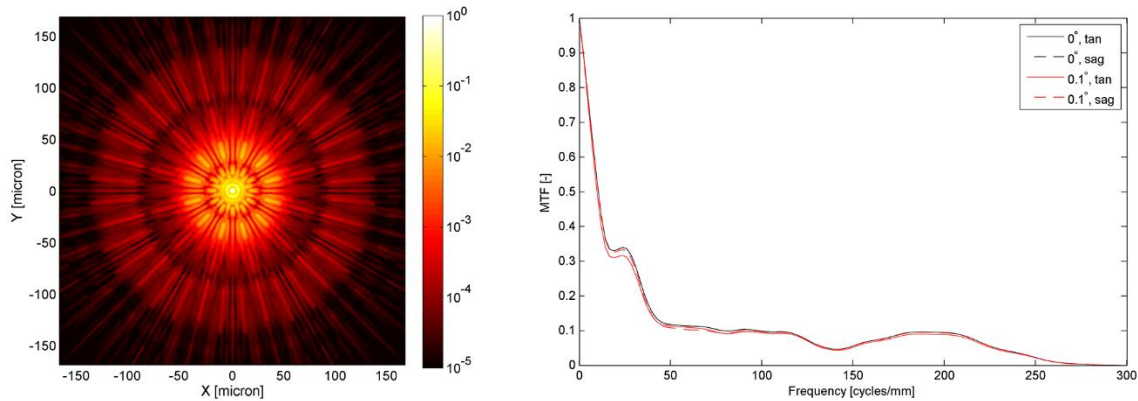


**Fig. 2:** Polychromatic Point Spread Function and MTF of the Michelson Synthetic Aperture

In Fig. 2, the optical performance of the Michelson Synthetic Aperture is shown. The point spread function is given for the most off-axis field, where the performance is worst. Both the polychromatic point spread function and the MTF curves show that the system delivers a nearly diffraction limited performance for the full field of view. A slight degradation in MTF is observed when going to the outermost fields, at field angles of  $\pm 0.1^\circ$ . However, this drop remains limited to just 3% at low spatial frequencies, while at higher frequencies almost no loss in resolving power is observed.

The full FOV that can be obtained with the Michelson system is limited to  $0.2^\circ$ , corresponding to a swath width of 1.75 kilometre. It falls short of the design goal of  $0.57^\circ$ , given in table 1. A small extension in the FOV may be achieved with the current optical design. However, to reach the FOV goal, a substantial redesign of the afocal telescopes is required.

### B. Fizeau Synthetic Aperture

Designing a Fizeau synthetic aperture system is a lot more straightforward, since its only difference compared to a conventional telescope is the shape of the entrance pupil. As a starting point for the concept, a full-field Korsch telescope was chosen for its compact size, good image performance and low distortions.

The primary mirror was split into three rectangular segments, which can be folded towards the instrument body during launch. The secondary mirror can be placed on an extendible boom, further reducing the stowed size of the instrument. The design was optimized for a short distance between the primary mirror segments and the secondary mirror, to reduce mechanical uncertainties in the extendible arm.

The number of primary mirror segments was selected following an MTF analysis. Even though an increase in the number of segments leads to a slightly higher MTF at the Nyquist frequency of the detector, this increase is accompanied by a loss in contrast at lower spatial frequencies. Additional advantages of using three segments are the more compact stowed volume of the instrument as well as the increased simplicity of the deployment mechanisms.

In Fig. 3 the optical lay-out of the Fizeau system is shown, while Fig. 4 on the next page shows the optical performance of the system.

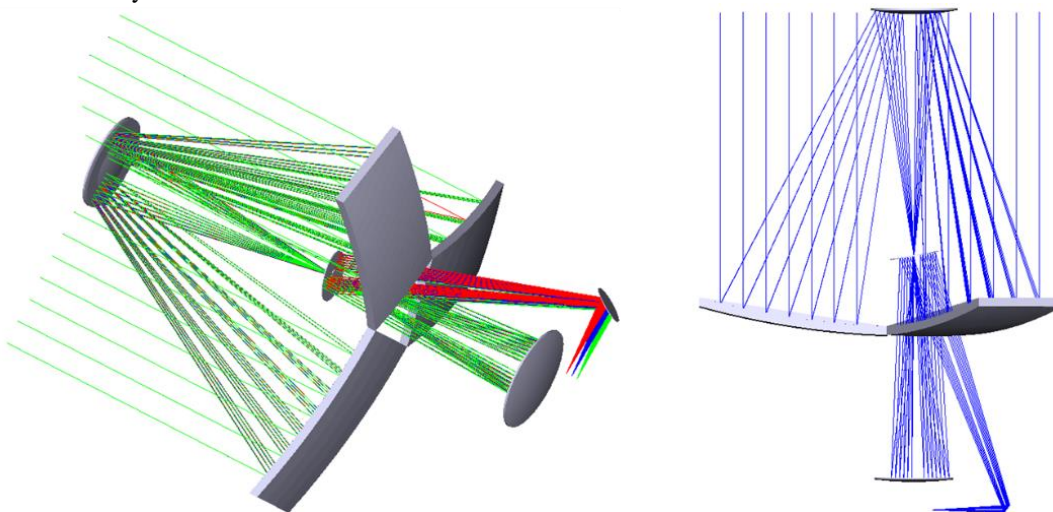


**Fig. 3:** Fizeau Synthetic Aperture

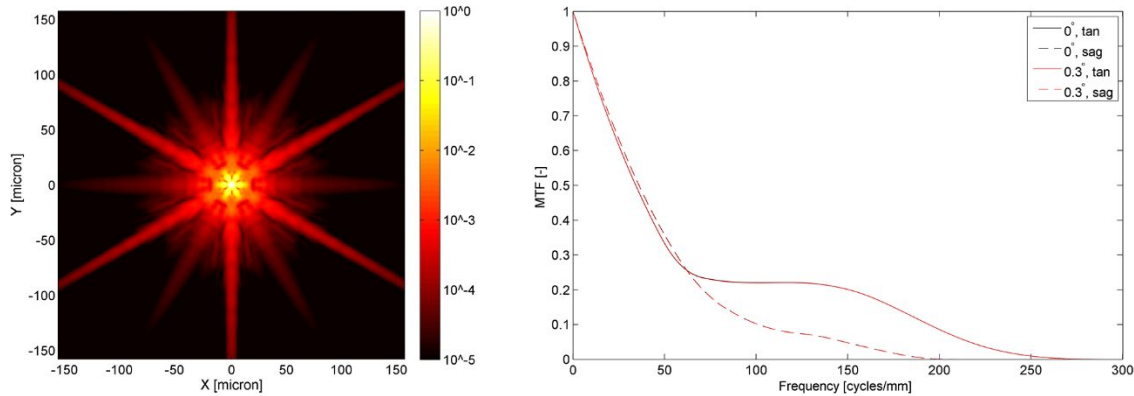


**Fig. 4:** Polychromatic Point Spread Function and MTF of the Fizeau Instrument

As shown in Fig. 4, the Fizeau synthetic aperture concept delivers a diffraction limited performance for the full field of view of  $0.6^\circ$ . The MTF curves for the centre and the edges of the field ( $\pm 0.3^\circ$ ) overlap for the full frequency range. There is a considerable variation in MTF depending on the direction, which is a logical consequence of the pupil configuration. However, for all spatial frequencies up till the Nyquist frequency of the detector (100 cycles/mm), the Fizeau system has a higher MTF than the Michelson system.

### C. Trade-off

A trade-off was performed between the two concepts. Below, a general description is given of the trade-off criteria and the relative performance of the concepts. A detailed description of the trade-off and the scoring systems that have been used are beyond the scope of this paper and is available for download at [5].

- **Stowed Size:** The stowed size was the most important criteria in this trade-off, as a compact launch volume greatly reduces the launch cost of the instrument and is a very important factor in bringing down the mass of the instrument. With a stowed volume of  $0.37 \text{ m}^3$ , calculated using CATIA, the Fizeau system is considerably more compact than the Michelson system, which has an estimated volume of  $1.06 \text{ m}^3$ . Note that both systems are substantially more compact than a conventional telescope designed for the same ground resolution. Such a system is estimated to have a volume of at least  $3.4 \text{ m}^3$ .
- **MTF:** The average MTF of both concepts was compared at the Nyquist frequency of the detector as well as half this frequency. As demonstrated in Fig. 3 and 4, at both spatial frequencies, the Fizeau system has a higher MTF and as such receives a higher score.
- **Effective Aperture Area:** For this trade-off the effective aperture was defined as the product of the total aperture area and the system transmission. The parameter can be seen as driving for achieving a good Signal-to-Noise (SNR) ratio. The Michelson system has substantially more optical elements in its optical path, resulting in a lower transmission, as well as a slightly smaller aperture area. Therefore, it receives a lower score.
- **Complexity:** The complexity of the two systems was compared on the basis of the number of optical components, the complexity of the surface types, the dimension of the largest optical component and whether or not the system uses moving parts. All in all, the complexity of the Fizeau system was determined to be lower than that of the Michelson system.
- **Field of View:** With a full field of view of  $0.6^\circ$ , the Fizeau system has a wider field of view than the Michelson system, which can only reach  $0.2^\circ$ . A further increase in field of view is possible for the Fizeau system, while large design changes are needed for the Michelson system.
- **Thermo-Mechanical Stability:** The thermo-mechanical stability of the Michelson is expected to be much more critical than that of the Fizeau system, primarily due to the long path lengths between the afocal telescopes and beam combiner as well as the large number of components. In addition, an active control system for the Michelson system will require the addition of several optical components, while for the Fizeau system direct actuation of the optical components is possible.
- **Straylight Sensitivity:** The Michelson system features multiple intermediate images, which can be used for the placement of a field stop and has small apertures that can be effectively baffled. While the Fizeau system also has a field stop, its aperture is much larger and therefore much more difficult to baffle. As such, the system is expected to be more sensitive to straylight.

In table 2, the results of the trade-off are presented. As shown, the Fizeau was a clear winner of the trade-off and was therefore used as the basis for further development.

**Table 2:** Trade-off between the Michelson and Fizeau systems. Scores between 0 and 5 were awarded for each trade-off criteria.

<i>Criteria</i>	<i>Weight</i>	<i>Michelson</i>	<i>Fizeau</i>
<i>Stowed Volume</i>	30	3	5
<i>MTF</i>	@ 50 mm <sup>-1</sup>	3	5
	@ 100 mm <sup>-1</sup>	2	4
<i>Effective Aperture Area</i>	20	2	3
<i>Complexity</i>	10	2.3	2.7
<i>Field of View</i>	8	2	5
<i>Thermo-mechanical Stability</i>	8	2	3
<i>Straylight Sensitivity</i>	4	4	2
<b>Weighted Average</b>		<b>2.5</b>	<b>4.0</b>

### III. DETAILED OPTICAL DESIGN AND SENSITIVITY ANALYSIS

Since the Fizeau concept already had a diffraction limited imaging performance, the changes that were made to the design after the trade-off were limited. A bit more clearance was created between the optical components and the beam to create more room for the support structure of the components. In addition, higher order terms were added to the description of the shape of the tertiary mirror to further improve the nominal wavefront quality.

In Table 3 below, a summary is given of some key performance parameters that can be obtained for the final optical design. The SNR values have been calculated for two lighting conditions under the assumption that a 128-stage TDI detector is used.

While the nominal optical performance of the deployable aperture telescope is excellent, this is by no means a guarantee for a good performance in the harsh and dynamic space environment. Therefore, a tolerance analysis has been performed. The main goal of this analysis was to create an alignment budget which must be met to ensure a good end-to-end image performance. It was determined experimentally that such a performance can be met, on the condition that the peak-to-valley wavefront error stays below 7 waves. If this condition is met, the passive calibration system to be described in section V of this paper can be used to retrieve the wavefront and correct the image.

In order to keep the wavefront error below the stated value, the elements must be positioned with the accuracies given in table 4. The directions of the axes used in this table are as follows: for the primary mirror segments, the X-axis is parallel to the long side of the segment, while the Y-axis is parallel to the short axis. The Z-axis for all optical elements is parallel to the optical axis of the telescope.

As can be seen, particularly for the primary mirror segments, the tolerances are very tight. Especially the tolerances on the positioning in the Z-direction and the tilts around the X- and Y-axis will be very challenging; it is clear that these values cannot be reached with a fully passive system. Underneath the primary mirror, actuators must therefore be placed to ensure that the tilt and piston error of the segments can be controlled.

The tolerances on the secondary and tertiary mirror are less challenging to meet. Even though the tolerances on the secondary mirror are outside the limits of a passive system, an active system is not foreseen here. The main reason is that the errors in its position can already be effectively compensated by the actuation system controlling the primary mirror segments.

**Table 3:** Key performance parameters of the final optical design

<b>Strehl Ratio</b>		> 0.99
<b>Optical MTF</b>	@ Nyquist (100 mm <sup>-1</sup> )	0.10 (s) / 0.23 (t)
	@ Half Nyquist (50 mm <sup>-1</sup> )	0.33 (s) / 0.32 (t)
<b>SNR</b>	Earth Reflectance: 0.3, Sun Zenith Angle: 60°	100
	Earth Reflectance: 0.5, Sun Zenith Angle: 23.5°	150

**Table 4:** Required position and orientation tolerances of the mirrors

<b>Element</b>	<b>Position [μm]</b>			<b>Tilt [μrad]</b>		
	<i>X</i>	<i>Y</i>	<i>Z</i>	<i>X</i>	<i>Y</i>	<i>Z</i>
Primary Mirror Segments	1	2	0.1	0.4	4.5	0.2
Secondary Mirror	4	4	2	17	17	50
Tertiary Mirror	10	10	5	17	17	50

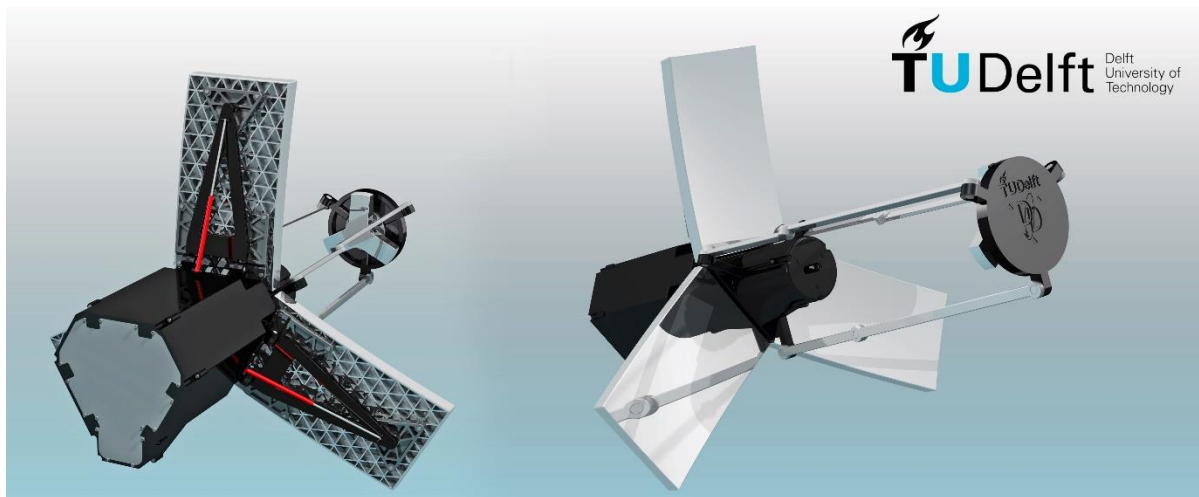


Fig. 5: Two views on the deployable aperture instrument

#### IV. MECHANICAL DESIGN

Using CATIA®, a conceptual mechanical design has been created for the deployable aperture telescope. In Fig. 5, two views on the instrument are shown. A compact and lightweight design has been created. In the stowed configuration, the design fills a hexagonal envelope with sides of 35 cm and a height of 1.1 meter. Currently, the nominal mass of the instrument is estimated to be 75 kg.

In the left view of Fig. 5, the back side of the lightweighted primary mirror panels is clearly shown. The mirror panels will be made using a Silicon Carbide (SiC) substrate. This material has been chosen on the basis of its low Coefficient of Thermal Expansion (CTE), high thermal conductivity, high stiffness and excellent lightweighting possibilities – as low as 7.1 kg/m<sup>2</sup> has already been demonstrated [6]. The low CTE of SiC makes the system quite tolerant to a thermal offset of one of the segments; thanks to the passive calibration system, a good performance can be achieved for a temperature range of up to  $\pm 5^\circ$  with respect to the desired operating temperature.

The primary mirror segments have been mounted on arms via three whiffles. Between the whiffles and the arms, actuators can be placed to control the tilt and vertical position of the mirror segments. The arms can fold downwards in the stowed configuration. Doing so, leads to the most compact stowed configuration. The arms are supported by an extending rod for additional stability during the measurements.

Not shown in Fig. 5 is the deployable baffle, which will be added to shield the instrument from straylight. During launch and integration of the satellite, the baffle will serve the additional purpose of shielding the sensitive reflective surface of the primary mirror segments from impacts.

The secondary mirror has been connected to the main housing via three deployable Invar arms. The arms feature a hinge in the centre to allow the mirror to be folded towards the main housing. Conceptually, the deployment mechanism of the secondary mirror is similar to that used in IXO, an X-ray observation telescope [7]. In the stowed configuration, the arms fit within the gap that is left when the primary are folded downwards. The arms have been positioned in such a way that they do not create any additional obscuration of the entrance pupil.

The main housing connects the primary and secondary mirror mechanisms to the other optical components. The temperature of the housing will be actively controlled to ensure that the displacements and deformations of all components within remain minimal.

In Fig. 6, the deployment sequence of the instrument is shown. The secondary mirror will deploy first, followed by the primary mirror segments. Since the speed of deployment is not critical, the deployment can be driven by motors placed on the hinges of the mechanisms.



Fig. 6: Deployment Sequence

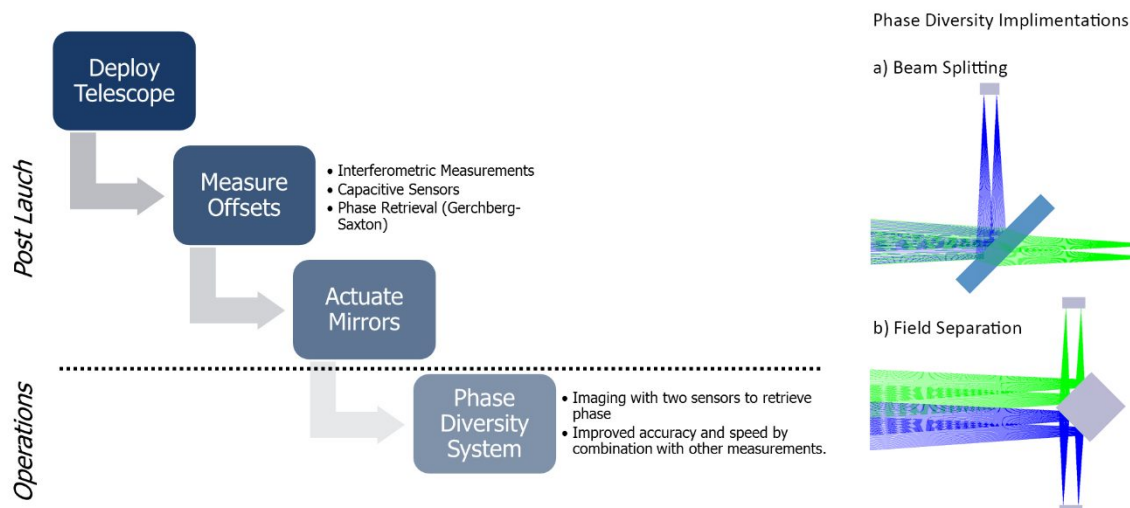


**Fig. 7:** Calibration strategy (left) and phase diversity implementations (right)

## V. CALIBRATION STRATEGY AND PHASE DIVERSITY

As shown in section IV, the deployable aperture system is very sensitive to misalignments of its optical elements. As such, a well-defined calibration strategy is of vital importance to ensure that a good image performance can be reached. In the left panel Fig. 7, a schematic overview is given of the proposed calibration strategy.

The calibration strategy can be split up into two phases. The first phase will occur directly after launch and may be repeated periodically to correct for long-term drifts. The main goal of this calibration phase is to ensure that the optical components are positioned with the accuracies defined in table 4. As an input to the calibration system, range measurements using capacitive sensors will be combined with interferometric measurements of a number of control points on the optical elements. In addition, measurements of stars can be used to estimate the wavefront errors of the telescope. To do so, wavefront retrieval algorithms, such as the Gerchberg-Saxton algorithm, can be used [8].

During operations, a phase diversity will be used to recover the residual wavefront error and subsequently correct the image. In a phase diversity system, two detectors are used to capture the same image. The second detector is placed at a known defocus distance with respect to the first detector. Phase diversity is based on the principle that there is a known difference between the generalized pupil function at the first detector and the second detector. The generalized pupil function  $H$  is given by (1) [9],

$$H_n(x, y) = P(x, y) \exp \left\{ j \frac{2\pi}{\lambda} (W(x, y) + W_{defocus}(x, y)) \right\}, \quad (1)$$

where  $P(x, y)$  is the binary pupil function,  $\lambda$  is wavelength and  $W(x, y)$  is the unknown wavefront which will be estimated.  $W_{defocus}(x, y)$  is the known defocus contribution to the wavefront; for the detector placed in the nominal focus, this term is equal to 0. To ensure a stable convergence in the presence of noise and a decrease in computing time, it is convenient to parameterize the wavefront by a set of aberration parameters  $\alpha$ . For this application, the wavefront coming from each of the three segments is parameterized with a set of 17 Zernike terms. It has been shown that by maximizing (2), an estimate can be obtained for the wavefront parameters [10].

$$L_m(\alpha) = - \sum_{u \in \chi} \frac{|D_1(u)S_2(u) - D_2(u)S_1(u)|^2}{|S_1(u)|^2 + |S_2(u)|^2} \quad (2)$$

$D_1$  and  $D_2$  in (2) are the Fourier transforms of the images obtained with the first and second detector, while  $S_1$  and  $S_2$  are the Fourier transforms of the estimates of the PSF at the first and second detector. The variable  $u$  is used for the spatial frequency. The summation is done over the set of spatial frequencies  $\chi$  within the passband of the instrument.

Two implementations of phase diversity were considered, as illustrated in the right panel of Fig.7. In the first approach, which is generally shown in literature, a beam splitter is placed close to the focal plane, reflecting half of the light to the second detector which is placed at a known defocus distance. In the second approach, the second detector is looking at a slightly different field than the primary detector.



**Fig. 8:** Results of the end-to-end simulation. Both images were obtained with field-separated phase diversity.

A major advantage of the second approach is that the two detectors do not need to share the light coming from the telescope, resulting in twice as much signal on the detector. One issue which could cause the phase retrieval to fail is that the unknown component of the wavefront is different at the two detector locations due to spatial variations. However, since both detectors will be placed very close to one another, this effect is expected to be very small, as was later confirmed by a Monte Carlo analysis.

To validate the principles of the phase diversity, an end-to-end analysis was performed using a combination of Zemax and Matlab modules. Perturbations were added to the optical model based on the budget given in table 4, after which wavefronts for both detectors were retrieved. The wavefronts were used to simulate the two images. Representative image noise was added before using the images in the phase diversity algorithms.

It was found that in 70% of the cases the wavefront was retrieved successfully and most detail lost due to misalignments was recovered. Besides this, the success rate of the algorithm was almost the same for the beam splitting implementation and the field separated implementation of phase diversity. It is expected that with future refinement of the algorithms, the success rate can be increased significantly. In Fig. 8 some results of this analysis are shown for two different scenes. The blurred pictures show the image quality, or the lack thereof, of a system with a peak-to-valley wavefront error of 6 waves. The recovered images have been obtained when deconvolving the blurry image using the retrieved wavefront.

## VI. CONCLUSIONS AND FUTURE WORK

Sub-meter resolution imagery has become increasingly important for disaster response, defence and security applications. This paper presents a promising concept for a deployable aperture instrument, delivering such images whilst using a fraction of the mass and volume compared to conventional telescopes. End-to-end performance simulations of the instrument and its calibration system show promising results. A good image quality was obtained, within the limitations of a synthetic aperture solution, despite inherent instabilities occurring in a deployable system. Future work will consist of the continuation of the mechanical design efforts and performing a detailed analysis of the thermo-mechanical stability of the system. Other topics that will be analysed in the near future are the metrology and actuation subsystems to be used in the post-launch calibration phase and a refinement of the phase diversity algorithms.

## REFERENCES

- [1] Digital Globe. "WorldView-3," 14-8-2014; Available from: <http://www.digitalglobe.com/about-us/content-collection#worldview-3>.
- [2] Mugnier, L., et al. "Multiple aperture optical telescopes: some key issues for Earth observation from a GEO orbit," in *5th International Conference on Space Optics (ICSO 2004)*. 2004. Toulouse, France
- [3] Rousset, G., et al., "Imaging with multi-aperture optical telescopes and an application," *Comptes Rendus de l'Académie des Sciences-Series IV-Physics*, 2001. 2(1): p. 17-25.
- [4] Stuhlinger, T.W. "All-reflective phased array imaging telescopes," in *1990 Intl Lens Design Conf.* 1991. International Society for Optics and Photonics.
- [5] Dolkens, D. "Trade-off between Fizeau and Michelson Synthetic Aperture," 2014; Available from: <http://www.spaceoptics.eu/docs/trade-off.pdf>.
- [6] Stahl, H.P., D.T. Leisawitz, and D.J. Benford. "Mirror requirements for SAFIR," in *Astronomical Telescopes and Instrumentation*. 2004. International Society for Optics and Photonics.
- [7] Bavdaz, M., et al. "IXO system studies and technology preparation," in *SPIE Optical Engineering+ Applications*. 2009. International Society for Optics and Photonics.
- [8] Fienup, J.R., "Phase retrieval algorithms: a comparison," *Applied optics*, 1982. 21(15): p. 2758-2769.
- [9] Harvey, J.E. and C. Ftaclas, "Field-of-view limitations of phased telescope arrays," *Applied optics*, 1995. 34(25): p. 5787-5798.
- [10] Paxman, R.G., T.J. Schulz, and J.R. Fienup, "Joint estimation of object and aberrations by using phase diversity," *JOSA A*, 1992. 9(7): p. 1072-1085.